applied sciences

MDPI

Article

Mechanical Properties of Basalt Fiber Reinforced Cemented Silty Sand: Laboratory Tests, Statistical Analysis and Microscopic Mechanism

Shuang Sun [1], Hanbing Liu [2], Chenglin Shi [1,*], Lina Xu [1] and Yongqiang Sui [3]

[1] School of Transportation Science and Engineering, Jilin Jianzhu University, Changchun 130118, China
[2] College of Transportation, Jilin University, Changchun 130012, China
[3] Haiwei Engineering Construction Co., Ltd., of Fhec of CCCC, Beijing 101119, China
* Correspondence: shichenglin@jlju.edu.cn; Tel.: +86-159-4303-4293

Abstract: Benefiting from low cost, high tensile strength, chemical stability, and great resistance to temperature, alkaline, and acids, it is a reasonable and valuable technology to use basalt fiber (BF) as an admixture to optimize building materials. So far, the challenge is still to master the engineering performance of BF-reinforced materials, especially poor subgrade soils. To this end, this paper carried out a series of unconfined compressive strength (UCS) tests, splitting tensile strength (STS) tests, and scanning environmental microscope (SEM) tests to study the mechanical properties and microstructure mechanism of BF-reinforced subgrade cemented silty sand with different fiber contents and curing times. The aims of this research were: (i) the UCS and STS of basalt fiber reinforced uncemented silty sand (BFUSM) and basalt fiber reinforced cemented silty sand (BFCSM) both increased with the increase of curing time and the strength reached the maximum value after curing for 28 days; (ii) the optimal fiber content was 0.2%, and a good linear correlation existed between UCS and STS; (iii) from the microscopic point of view, the combination of BF and cement could combine the physical action of fiber reinforcement and the chemical action of cement hydration reaction to form a fiber-cement-soil skeleton structure to improve the strength of silty sand and the improvement effect after working together was better than separately incorporated BF or cement; and (iv) the corresponding developed multiple nonlinear regression (MNLR) models which can well predict UCS and STS of BFUSM and BFCSM were established.

Keywords: basalt fiber reinforced cemented silty sand (BFCSM); unconfined compressive strength (UCS); splitting tensile strength (STS); microscopic mechanism; multiple nonlinear regression (MNLR) models

Citation: Sun, S.; Liu, H.; Shi, C.; Xu, L.; Sui, Y. Mechanical Properties of Basalt Fiber Reinforced Cemented Silty Sand: Laboratory Tests, Statistical Analysis and Microscopic Mechanism. *Appl. Sci.* **2023**, *13*, 3493. https://doi.org/10.3390/app13063493

Academic Editor: Muhammad Junaid Munir

Received: 14 February 2023
Revised: 6 March 2023
Accepted: 7 March 2023
Published: 9 March 2023

1. Introduction

The unconfined compressive strength (UCS) test was used to verify the effectiveness of cement stabilization or to understand the importance of factors affecting the strength of cemented soil, which is widely used due to its convenient parts and simple testing. UCS has been recommended by the American Society for Testing and Materials as a standard guide and quantitative indicator for evaluating the effectiveness of the improvement. With the development of soil mechanics, splitting tensile strength (STS) has gradually become an effective method for evaluating the improvement effects of soil [1–3].

Silty sand is a rich reserved subgrade material in the northeast of China, which has many disadvantages, such as low natural water content, small plasticity index, weak shear strength, etc. These characteristics make it difficult to compact during construction, and it is prone to large deformation under loading, resulting in serious subgrade diseases for road constructed with the material, reducing the service life of the road [4–10]. Therefore, to reinforce the subgrade silty sand to meet performance requirements before use becomes particularly valuable.

Stable soil can meet the needs of engineering technology and is widely used in geotechnical engineering. In the past, most of the domestic and foreign choices focused on stabilizers made of inorganic binder materials, such as cement, lime, and fly ash, and the properties of the stabilized soil are already mature and reliable through numerous research, which could provide guidance for construction and be widely used in the treatment of soft foundations and road and railway foundations [11–15]. As we all know, the stabilizing effects of cement are better among inorganic binder materials [16–18]. However, cement is one of the many causes the CO_2 emissions [19]. As a result, attention to fiber-reinforced cemented soil has arisen in recent years.

The relevant literature has already confirmed that the incorporation of fiber will give the soil better physical and mechanical properties [20–26]. For fiber reinforcement, the common fiber types are basalt fiber (BF), polypropylene fiber, glass fiber, lignin fiber, cornsilk fiber, and carbon fiber. Among these, BF as an economical and environmentally friendly inorganic material, produced by melting and stretching natural volcanic basalt rock at 1450~1500 °C, has many advantages, such as high tensile strength and chemical stability. Moreover, BF is cheaper than glass fiber or carbon fiber since it is consumed less and has no additives [27,28]. Furthermore, the chemical properties of BF are similar to that of cement, thus the bond strength between them is better [29]. Therefore, it has been widely used to reinforce the mechanical properties of concrete and asphalt concrete [30–35]. Similarly, the incorporation of BF can also contribute to improving the strength properties of plain soil and cemented soil, which enhances the bonding between the particles and the fibers and weaken the void ratio. Furthermore, the improvement effect of the cement and fiber combination is better than the effect of only incorporated BF or cement [36,37]. Meanwhile, fiber content is an important factor affecting the mechanical properties of reinforced soil, which affect the formation of the fiber–soil net [38]. Ndepete and Sert [39] concluded that the shear strength of BF-reinforced silty soil increased as the fiber contents increased. With a fiber content of 1.5% and a fiber length of 24 mm, the strength had the largest improvement. Gao et al. [40] suggested that the best improvement effect of BF-reinforced clay was obtained at 0.25% fiber content and 12 mm fiber length. The clay had the "poststrong" characteristic after the incorporation of fiber. Cao et al. [41] found that the reinforced soil had better mechanical properties with the inclusion of 10% fly ash and 0.6% BF after incorporating 5% cement. The UCS of reinforced soil first increased and then decreased with the increase in fiber contents. The BF could fill particles well to improve strength from SEM images. Wang et al. [37] proposed that the UCS and peak deviator stress of cement-solidified kaolinite obtained the highest value at 0.2% and 0.4% BF content, respectively. A well-interconnected skeletal structure formed by the combination of fiber and cement was the main reason for the increase in strength derived from SEM. Wang et al. [26] considered that the UCS of BF-reinforced geopolymer-stabilized clay increased first and then decreased with the increasing fiber contents and fiber lengths. The best fiber content was 0.4% and the most suitable fiber length was 12 mm.

However, most of these studies have paid more attention to the mechanical properties of BF-reinforced cemented clay and neglected the other widely reserved subgrade soil-silty sand. Furthermore, research on fiber-strengthening mechanisms is limited. In summary, more attention should be given to the mechanical properties and the mechanism of BF-reinforced subgrade soil, especially in BF-reinforced cemented subgrade silty sand.

Therefore, BF-reinforced cemented silty sand (BFCSM) was selected as the research object. The aim of the paper is to clarify the effect of BF on the mechanical properties of cemented silty sand and reveal the corresponding fiber-reinforced microstructural mechanisms. To better investigate the effects of fiber contents and curing time, a series of UCS tests and STS tests are conducted on BF-reinforced uncemented silty sand (BFUSM) and BFCSM, and a series of developed MNLR models are established to predict UCS and STS. Simultaneously, the corresponding microstructure images are obtained by SEM tests, so as to explore the reinforced mechanism of BF incorporation. Finally, the purpose of this study

is to propose an innovative combination of BF with cement to enhance the strength of silty sand and provide a reliable reference for subgrade improvement engineering.

2. Materials and Test Programs

2.1. Materials

The subgrade silty sand was obtained from Songyuan County of Jilin Province. The particle analysis test results and the basic physical properties of cemented silty sand are presented in Figure 1 and Table 1, respectively, based on the Chinese specification of JTG 3430-2020, Test Methods of Soils for Highway Engineering [42]. Based on the previous research of our team, the optimal cement content of stabilized silty sand is a 2% dosage [43]. The cement content is measured by the percentage of cement in the mass of the dry soil, as Chen et al. [44] proposed. From Table 1, the initial water content of plain soil is 5.47%. The specific gravity obtained by the pycnometer test is 2.68. The liquid limit and plastic limit are obtained by the liquid–plastic limit combined test method. The optimum water content of plain soil is 8.53% and that of cemented soil is 9.69%. The maximum dry density of them, which was tested by the heavy compaction test, is 2.030 g/cm^3 and 2.042 g/cm^3, respectively. The coefficient of uniformity, C_u, and coefficient of curvature, C_c, of plain soil are 5.8 and 1.33, respectively. In summary, the plain soil is a well-graded low liquid limit silty sand classified by the Chinese specification of JTG 3430-2020.

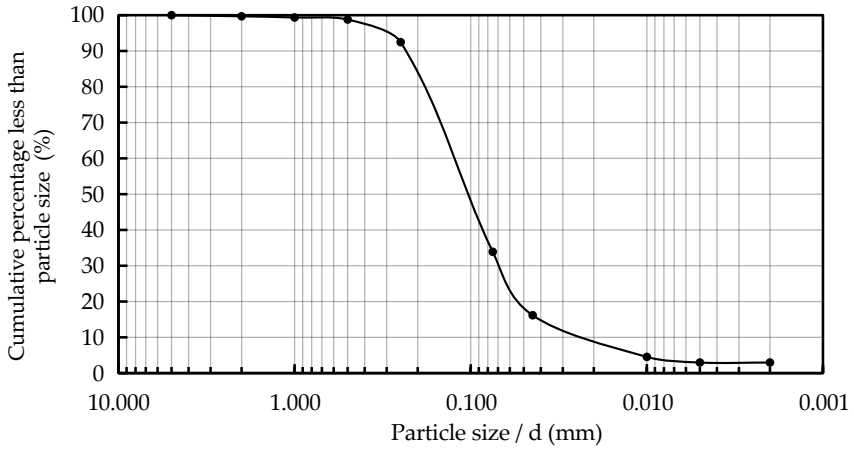

Figure 1. Particle size distribution curve of silty sand.

Table 1. The basic physical properties of silty sand and cemented silty sand.

Parameters	Silty Sand	Cement Reinforced Silty Sand
Cement content (%)	0	2
Initial water content w (%)	5.47	4.17
Specific gravity	2.68	-
Liquid limit w_L (%)	22.4	26.6
Plastic limit w_P (%)	14.1	17.6
Plasticity index I_P (%)	8.3	8.9
Optimum water content w_{opt} (%)	8.53	9.69
Maximum dry density ρ_d (g/cm^3)	2.030	2.042
Coefficient of uniformity C_u (%)	5.8	-
Coefficient of curvature C_c (%)	1.33	-

The cement used in this study is Portland cement (P.O 42.5) produced by Yatai Cement Co., Ltd., of Jilin Province (Changchun, China). The chopped BF used as Figure 2 shows, has a monofilament length of 12 mm obtained from Anjie Composite Material Co., Ltd., of Zhejiang Province (Haining, China). The physical properties of BF are given in Table 2. The diameter of BF is 7~15 μm. The density is 2.63 g/cm^3, similar to the maximum dry

density of cemented silty sand. The tensile strength, elastic modulus, and melting point of monofilament of BF are 3000~4800 Mpa, 91~110 Gpa, and 1050 °C, respectively. Those mentioned data manifest that fiber has great mechanical properties and great resistance to temperature.

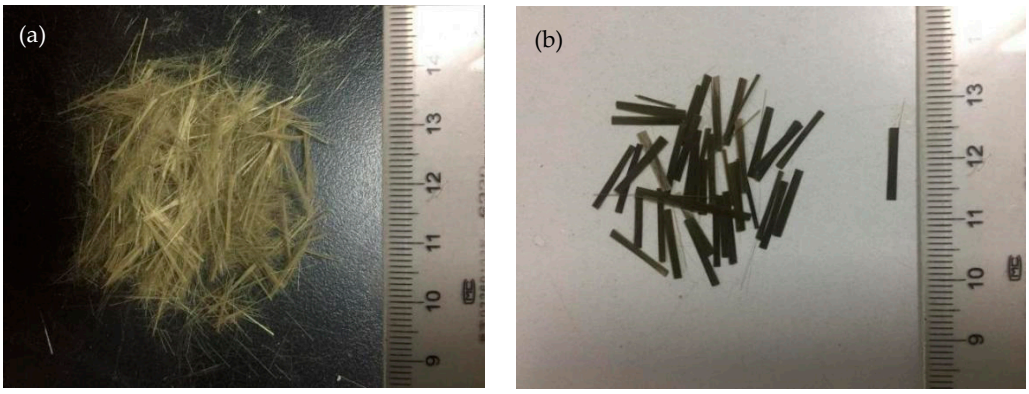

Figure 2. Basalt fibers used in this study: (**a**) dispersed fiber, and (**b**) clustered fiber.

Table 2. The performance indicator of basalt fibers.

Parameter	Fiber Type	Diameter (μm)	Density (g/cm^3)	Tensile Strength (MPa)	Elastic Modulus (Gpa)	Melting Point (°C)
Value	Monofilament	7~15	2.63	3000~4800	91~110	1050

2.2. Test Programs

2.2.1. Sample Preparation

The UCS tests and STS tests both used the cylinder samples prepared in laboratories, with a diameter of 50 mm and a height of 100 mm with optimum water content, according to the impact molding method of the Chinese specification of JTG 3430-2020, the reason for using optimum water content to mold the samples is that the BF did not absorb water [45]. The fiber length selected was 12 mm [37] and unreinforced soil was taken as a comparison. Each condition is molded with five different BF contents: 0.0%, 0.1%, 0.2%, 0.3%, and 0.4% [37], where the fiber content is measured by the percentage of fiber in the total mass of the soil and cement. First, the appropriate water was added to the silty sand until it reached the optimum water content by a mechanical mixer, then stored in an airtight container for 24 h to make the internal water distribute uniformly. Subsequently, incorporating cement and BF into the prepared soil and mixed for 10 min by a mechanical mixer. Thereafter, the blend was compacted at the lowest (minimum 96%) compaction standard of high-grade highway subgrade material. After being molded, each sample was tightly packaged with plastic wrap to prevent water dispersion and evaporation during curing and to block external water sources. Then, according to the Chinese specification of JTG E51-2009, Test Methods of Materials Stabilized with Inorganic Binders for Highway Engineering [46], packaged samples were placed into a curing room with a temperature of 20 ± 2 °C and a relative humidity greater than 95% for 3 days, 7 days, 14 days, and 28 days. The preparation process is illustrated in Figure 3.

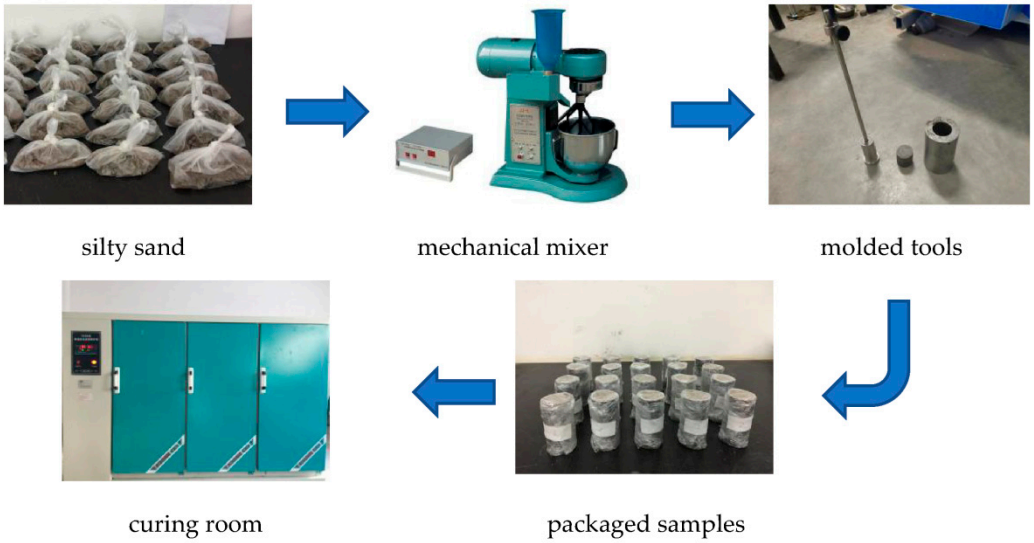

Figure 3. Samples molded and curing process.

The blend design for exploring the effects of BF on cemented silty sand is displayed in Table 3. Group 1 is BFUSM, which is a reference to make a comparison with BFCSM (Group 2). The UCS tests and STS tests need a minimum of six samples molded with the same properties are tested to obtain the typical of data (three for compression and three for splitting), then the mean value of the three data is defined as the value of UCS (q_u) and STS (q_t).

Table 3. The summary of test schemes.

Types of Tests	Group	Blend Name	BF Content (%)	BF Length (mm)	Curing Time (Days)
UCS test/ STS test	1	SM0B	0.0	-	3, 7, 14, 28
		SM0.1B	0.1	12	3, 7, 14, 28
		SM0.2B	0.2	12	3, 7, 14, 28
		SM0.3B	0.3	12	3, 7, 14, 28
		SM0.4B	0.4	12	3, 7, 14, 28
	2	SM2P0B	0.0	-	3, 7, 14, 28
		SM2P0.1B	0.1	12	3, 7, 14, 28
		SM2P0.2B	0.2	12	3, 7, 14, 28
		SM2P0.3B	0.3	12	3, 7, 14, 28
		SM2P0.4B	0.4	12	3, 7, 14, 28

Note: Silty sand abbreviated to SM, P represents Portland cement, and B represents basalt fiber.

2.2.2. UCS Test

The samples prepared for UCS tests are listed in Table 3. A universal testing machine (Figure 4a) with a maximum load sensor of 100 kN, measuring error of ±1%, and control precision of ±0.5%, was used. The vertical constant loading displacement rate of 1 mm/min is applied to the sample until it failed. Then q_u could be calculated by Equation (1).

$$q_u = \frac{P}{\pi R^2} \quad (1)$$

where q_u is the value of UCS (Mpa), P is the maximum vertical loading pressure (kN), and R is the radius of the cylinder (mm).

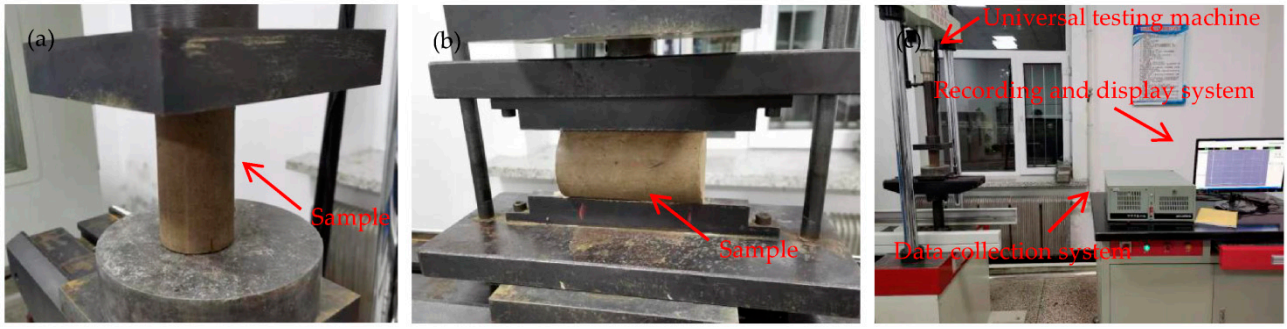

Figure 4. Universal testing machine used for tests: (**a**) UCS test, (**b**) STS test, and (**c**) test system.

2.2.3. STS Test

The STS tests followed the Chinese specifications of JTG 3430-2020. The automatic loading machine, samples, and vertical constant loading displacement rate performed on the STS tests are the same as the UCS tests (Figure 4b). Thereafter, q_t could be obtained by Equation (2).

$$q_t = \frac{2P}{\pi LD} \quad (2)$$

where q_t is the value of STS (Mpa), P is the maximum vertical loading pressure (kN), and L and D are the length and diameter of the cylinder (mm), respectively.

2.2.4. SEM Test

The SEM test is conducted to clearly figure out the mechanism of reinforced BF. The samples used in the SEM test are the samples of BFUSM and BFCSM after UCS tests. First, cut the fresh undisturbed surface into small pieces with the size of 10 × 10 × 10 mm. Subsequently, the cut samples were put in the oven at a temperature of 50 °C to dry them to a constant weight. Then, the dried samples were adhered to the SEM observation table with conductive tape, followed by vacuuming and spraying gold to make them conductive. Finally, the microscopic morphological images of silty sand before and after the incorporation of fiber and cement could be observed by the Field emission environmental scanning electron microscope XL-30, as Figure 5 showed.

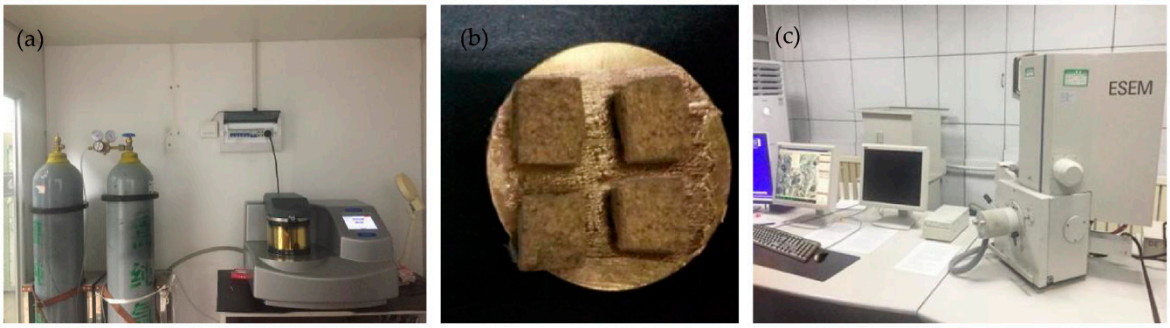

Figure 5. SEM test system: (**a**) vacuum treatment, (**b**) gold spray treatment and (**c**) scanning electron microscope XL-30.

3. Results

3.1. UCS

Figure 6 shows the UCS of BFUSM and BFCSM at varying BF contents and curing times with a length of 12 mm. It is obvious that the UCS of BFUSM and BFCSM both have an increasing trend as curing time increases and reach the maximum strength after curing for 28 days. Without the incorporation of cement (Figure 6a), the fiber content increases from 0.0% to 0.1% and 0.2%, the corresponding strength is 0.45 Mpa, 0.48 Mpa, and 0.67 Mpa, respectively. Thereafter, the fiber content increases to 0.3% and 0.4% and the

strength a small decrease to 0.46 Mpa and 0.49 Mpa, respectively. It can be found that at the fiber content of 0.2%, the UCS of BFUSM is the highest. The reason is that when fiber content is higher than 2%, the pull-out effect of fiber is significant, resulting in lower UCS. Hence, a 0.2% dosage is more suitable to reinforce BFUSM. The UCS of SM0.2B at 3 days, 7 days, 14 days, and 28 days is 0.32 Mpa, 0.56 Mpa, 0.60 Mpa, and 0.67 Mpa, respectively. The increasing amplitude of adjacent curing time is 75.61%, 5.77%, and 12.04%, indicating that the UCS of SM0.2B increases the most after curing for 7 days.

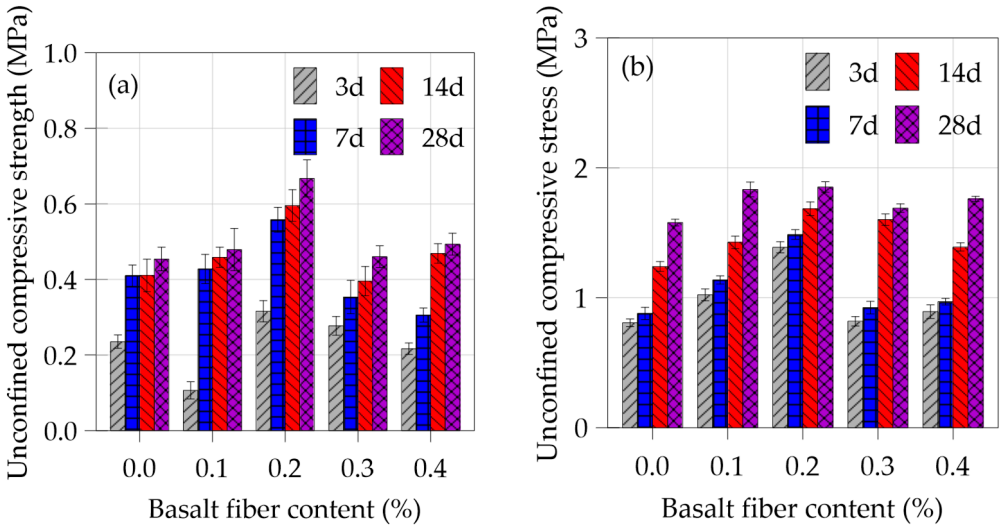

Figure 6. Unconfined compressive strength of reinforced silty sand at varying BF contents and curing times with a length of 12 mm: (**a**) BFUSM and (**b**) BFCSM.

As Figure 6b presented, the UCS of BFCSM increases first and then decreases with the increasing fiber contents, which is coincident with the conclusions of Cao et al. [41]. The UCS of SM2P0B is 1.58 Mpa, the corresponding UCS of SM2P0.1B, SM2P0.2B, SM2P0.3B, and SM2P0.4B is 1.16 times, 1.17 times, 1.07 times, and 1.12 times that of SM2P0B, manifesting that BFCSM reaches the maximum strength at 0.2% dosage, which is the optimal dosage for BFCSM. Since the fiber content is higher than 2% dosage, the pull-out effect of fiber is obvious under compressing, which leads to a decrease in strength. The UCS of SM2P0.2B at 3 days is 1.39 Mpa, the corresponding strength at 7 days, 14 days, and 28 days is 1.07 times, 1.21 times, and 1.33 times that at 3 days, the increasing amplitude between adjacent curing time is 7.16%, 13.22%, and 10.00%, respectively, implying that the UCS of SM2P0.2B has the maximum increasing amplitude after curing for 14 days.

Comparing Figure 6a and 6b, the UCS of BFCSM is obviously higher than that of BFUSM at the same fiber content and curing time condition [37,47,48]. The UCS of SM2P0.2B at 3 days, 7 days, 14 days, and 28 days is 3.39 times, 2.67 times, 2.83 times, and 2.78 times that of SM0.2B, indicating that the cementation effect of hydration reaction is more significant than that of BF on UCS, the reason is that BFUSM relies on the fiber to "build bridges" between particles to increase UCS of soil. But in BFCSM, the fiber "build bridges" in the cement-soil skeleton, which makes particles more closely connected and leads to a significant increase in strength [40]. The multiple relationships between the UCS of SM0.2B and SM2P0.2B remain basically unchanged after curing for 14 days, indicating that after the inclusion of cement, the increasing impact on UCS of the combined action of fiber and cement tends to be stable after 14 days of curing.

3.2. STS

Figure 7 displays the STS of BFUSM and BFCSM at varying BF contents with a length of 12 mm after curing for different days. We can find that the STS of BFUSM and BFCSM both increase with curing time and reach the maximum strength after curing for 28 days. As

Figure 7a showed, the STS of BFUSM at 28 days decreased from 0.052 Mpa to 0.044 Mpa as the fiber content increased from 0.0% to 0.1%. The maximum STS is 0.074 Mpa obtained at a 0.2% dosage. Thereafter, the STS decreased from 0.074 Mpa to 0.054 Mpa and 0.050 Mpa with the increase in fiber contents. Figure 7b shows that the STS of BFCSM at 28 days increased first and then decreased as fiber contents increased. The STS of BFUSM and BFCSM decreased at the fiber content of 0.3% or more, since with the increasing fiber content, the fiber agglomeration effect is enhanced, resulting in a decrease in strength. The 2% dosage is the tipping point where agglomeration is highlighted. The STS of BFCSM, without the incorporation of fiber, is 0.192 Mpa, the corresponding strength of SM2P0.1B~SM2P0.4B is 1.19 times, 1.30 times, 1.22 times, and 1.08 times that of SM2P0B. From the above, the maximum STS of BFCSM appears at 0.2% dosage, meaning the fiber content of 0.2% is more appropriate to reinforce cemented silty sand.

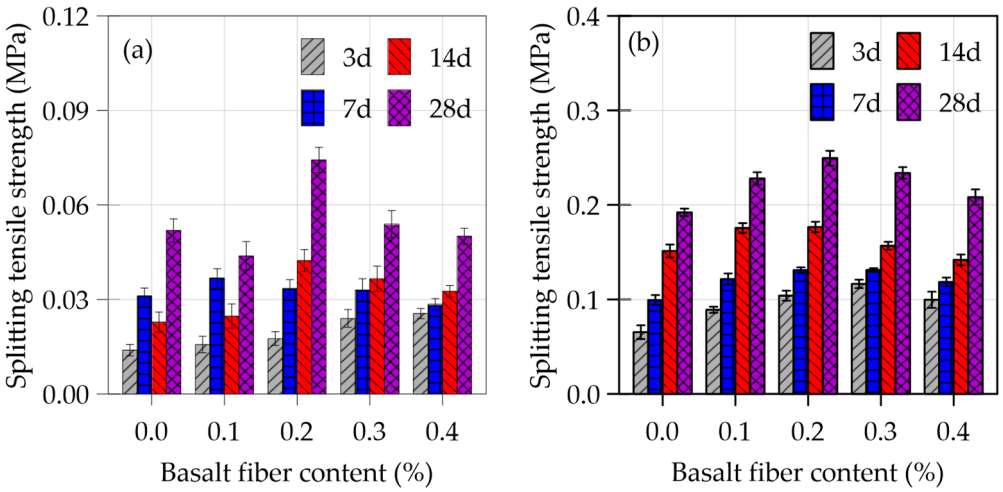

Figure 7. Splitting tensile strength of reinforced silty sand at varying BF contents and curing time with a length of 12 mm: (**a**) BFUSM and (**b**) BFCSM.

When the fiber content is 0.2%, the maximum increasing amplitude of SM0.2B and SM2P0.2B is 74.60% and 41.29%, which are both obtained after curing for 28 days. The corresponding STS of SM2P0.2B at 3 days, 7 days, 14 days, and 28 days are 4.91 times, 3.91 times, 4.17 times, and 3.36 times that of SM0.2B, indicating that STS of BFCSM is significantly increased compared to that of BFUSM. At the same time, comparing the increasing amplitude of STS and UCS under the same conditions, the increase of STS is greater than UCS under the combined action of fiber and cement and is the reason that fiber has good toughness and tensile ability.

3.3. Correlation between UCS and STS

The correlation between UCS and STS of both BFUSM and BFCSM at varying fiber contents and curing time with a length of 12 mm are shown in Figure 8.

Figure 8 manifests that the UCS and STS of BFUSM and BFCSM have a good linear correlation, which is coincident with the conclusion of Tran et al. [49,50]. The correlation coefficient of the UCS and STS of BFUSM is 0.802, while that of BFCSM is 0.912, showing that the inclusion of cement enhances the correlation between the UCS and STS. The relationship coefficients between the UCS and STS of BFUSM and BFCSM are 0.093 and 0.149, respectively, which had good similarity with Xiao et al. [36]. Hence, the relationship between the UCS and STS of BFUSM and BFCSM could be expressed by Equations (3) and (4).

$$q_{tBFUSM} = 0.093 q_{uBFUSM} - 0.002 \quad (3)$$

$$q_{tBFCSM} = 0.149 q_{uBFCSM} - 0.040 \quad (4)$$

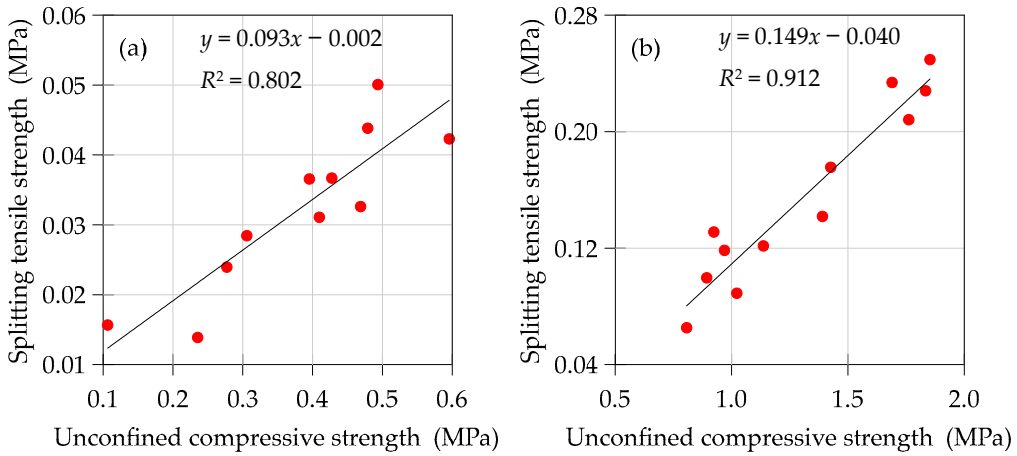

Figure 8. Correlation between unconfined compressive strength and splitting tensile strength: (**a**) BFUSM and (**b**) BFCSM.

4. Statistical Analysis of Multiple Factors

4.1. Multiple Nonlinear Regression Models

Considering the effect of BF contents and curing time, based on the research of Ahmed [51], Maliakal, and Thiyyakkandi [52], the multiple nonlinear regression (MNLR) models are adopted to predict UCS (q_u) and STS (q_t) of BFUSM and BFCSM with a length of 12 mm, the form of established MNLR models as Equation (5) showed:

$$Y = K_0 + K_1X_1 + K_2X_2 + K_3X_1^2 + K_4X_2^2 + K_5X_1X_2 \quad (5)$$

where Y is the dependent variable, the output variable (UCS (q_u), or the STS (q_t)), X_1 and X_2 are the independent variables or input variables, defied as BF contents (B) and curing time (D), respectively. K_0~K_5 are the regression coefficients, which solve the matrix form that consists of the independent variables and the dependent variables.

Thereafter, the coefficient of determination R^2 and the P-values of each variable are obtained to confirm the reliability of the MNLR models. Meanwhile, the reviewed MNLR models are developed based on the initial regression models, which is more suitable to predict q_u and q_t. R^2 represents the relationship between the observed data and the predicted data. The p-values of coefficients (K_1~K_5) corresponding to each variable in Equation (5) should be less than 0.05 to indicate strong evidence against the null hypothesis ($K_1 = K_2 = \ldots = K_5 = 0$). Then, the final developed MNLR models are determined.

4.2. Statistical Analysis

The MNLR models for predicting q_u of BFUSM and BFCSM with varying factors based on 120 experiment data points are obtained as Equations (6) and (7) showed, respectively.

$$q_{uBFUSM} = 0.2191 + 0.0892B + 0.0231D - 0.5663B^2 - 0.0005D^2 + 0.0076BD,\ R_a^2 = 0.824 \quad (6)$$

$$q_{uBFCSM} = 0.5295 + 1.4716B + 0.0691D - 3.3955B^2 - 0.0011D^2 + 0.0069BD,\ R_a^2 = 0.919 \quad (7)$$

$$q_{uBFCSM\text{-}R} = 0.1968 + 0.0246D - 0.0005D^2 + 0.0009BD,\ R_a^2 = 0.821 \quad (8)$$

$$q_{uBFCSM\text{-}R} = 0.5892 + 0.0693D - 0.0011D^2 + 0.0128BD,\ R_a^2 = 0.907 \quad (9)$$

The R_a^2 value of MNLR models for BFUSM and BFCSM is 0.824 in Equation (6) and 0.919 in Equation (7), respectively, implying that fiber contents and curing time are relevant to q_{uBFUSM} and q_{uBFCSM}. However, the P-values of coefficients with B and B^2 are larger than 0.05 as Table 4 showed, manifesting that the variables of B and B^2 have nothing to do with q_{uBFUSM} and q_{uBFCSM}, thus the two variables should be eliminated. Therefore, the developed MNLR models are obtained in Equations (8) and (9), respectively. It is

obvious that the coefficients of variable *BD* in the developed MNLR models are 0.0009 and 0.0128, respectively, showing that the interaction between fiber contents and curing time on the UCS is significant. Simultaneously, the *p*-values of the coefficients associated with variables which are both less than 0.05 as Table 4 displayed, indicating the effectiveness of the developed models. Meanwhile, the experimental data and the predicted data have a good relationship, as Figure 9 displayed, implying that the developed MNLR models are more reasonable to predict q_{uBFUSM} and q_{uBFCSM}.

Table 4. The *p*-values of coefficients corresponding to variables in MNLR models for predicting q_u.

Variables	*p*-Value		Revised *p*-Value	
	q_{uBFUSM}	q_{uBFCSM}	$q_{uBFUSM\text{-}R}$	$q_{uBFCSM\text{-}R}$
Intercept	3.9460×10^{-2}	1.1580×10^{-2}	2.9160×10^{-2}	9.7400×10^{-3}
B	2.6642×10^{-2}	7.5441×10^{-1}	-	-
D	5.2200×10^{-2}	1.5680×10^{-2}	5.0500×10^{-3}	1.6160×10^{-2}
B^2	6.3554×10^{-1}	1.7804	-	-
D^2	1.5274×10^{-4}	4.4604×10^{-4}	1.5329×10^{-4}	4.7835×10^{-4}
BD	6.6200×10^{-3}	1.8610×10^{-2}	3.8400×10^{-3}	1.1600×10^{-2}

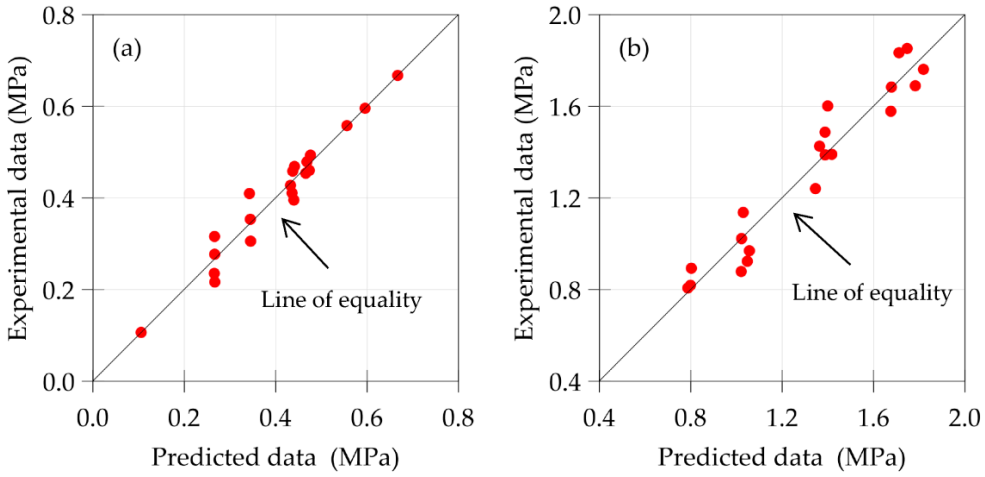

Figure 9. Relationship between experimental data and predicted data with a length of 12 mm for UCS: (**a**) BFUSM and (**b**) BFCSM.

Similarly, the MNLR models for predicting STS of BFUSM and BFCSM with a length of 12 mm based on 120 experimental data points are shown in Equations (10) and (11), respectively.

$$q_{tBFUSM} = 0.0090 + 0.0249B + 0.0030D - 0.0535B^2 - 0.0001D^2 - 0.0004BD,\ R_a^2 = 0.859 \quad (10)$$

$$q_{tBFCSM} = 0.0470 + 0.3629B + 0.0074D - 0.7531B^2 - 0.0001D^2 - 0.0020BD,\ R_a^2 = 0.967 \quad (11)$$

$$q_{tBFUSM} = 0.0090 + 0.0102B + 0.0030D - 0.0001D^2 - 0.0006BD,\ R_a^2 = 0.880 \quad (12)$$

$$q_{tBFCSM} = 0.0621 + 0.0616B + 0.0074D - 0.0001D^2 - 0.0020BD,\ R_a^2 = 0.971 \quad (13)$$

The R_a^2 value of MNLR models for BFCSM (0.967 for Equation (11)) is higher than that for BFUSM (0.859 for Equation (10)), indicating that the correlation between fiber contents, curing time, and q_{tBFCSM} is better than that with q_{tBFUSM}. The influence of variables on q_{tBFCSM} is more evident. However, the *p*-value of coefficients associated with B^2 is larger than 0.05 in Table 5, showing that the variables of B^2 could be eliminated. Therefore, the developed MNLR models are displayed in Equations (12) and (13), respectively. From Equations (12) and (13), the coefficients of variable *BD* in the developed models are 0.0006 and 0.0020, respectively, manifesting that the interaction between fiber contents and curing

time on the STS is significant. Meanwhile, the R_a^2 value in the developed models is a little higher than the initial models and the p-values of coefficients corresponding to variables are both less than 0.05 in Table 5, showing that the developed models predict the STS more ideally. At the same time, the relationship between experimental data and predicted data is good as Figure 10 displayed, illustrating that the developed MNLR models are more suitable to predict q_{tBFUSM} and q_{tBFCSM}.

Table 5. The p-values of coefficients corresponding to variables in MNLR models for predicting q_t.

Variables	p-Value		Revised p-Value	
	q_{tBFUSM}	q_{tBFCSM}	$q_{tBFUSM\text{-}R}$	$q_{tBFCSM\text{-}R}$
Intercept	5.3200×10^{-3}	8.4900×10^{-3}	4.9000×10^{-3}	1.4690×10^{-2}
B	4.7610×10^{-2}	5.6730×10^{-2}	2.1530×10^{-2}	4.6050×10^{-2}
D	9.3278×10^{-4}	1.1300×10^{-3}	8.2574×10^{-4}	2.0500×10^{-3}
B^2	1.5194×10^{-1}	1.2681×10^{-1}	-	-
D^2	2.9044×10^{-5}	3.3268×10^{-5}	2.5499×10^{-5}	6.0297×10^{-5}
BD	1.2900×10^{-3}	1.5800×10^{-3}	1.0700×10^{-3}	2.8600×10^{-3}

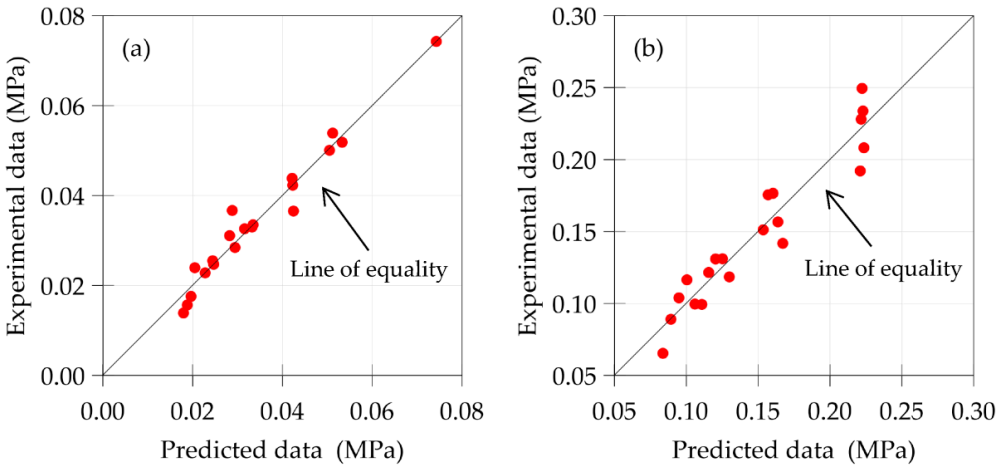

Figure 10. Relationship between experimental data and predicted data with a length of 12 mm for STS: (**a**) BFUSM and (**b**) BFCSM.

5. Microscopic Mechanism of Fiber Reinforcement

From the above, we knew that both the UCS and STS of BFCSM are better than that of BFUSM. The changes in macromechanical properties are obvious, however, the reasons for the changes are not clear. Therefore, the microscopic images of SM0B, SM0.2B, SM2P0B, and SM2P0.2B after curing for 14 days are displayed in Figure 11 to explore the reasons for mechanical properties changes.

From Figure 11a, with no fiber and cement incorporated, the formation of soil strength only depends on the bonding force between particles. The pores are large. The structure is a "honeycomb structure". The ability of interparticle bonding is poor, which leads to low strength. The schematic diagram as Figure 12a is presented.

When BF is incorporated, the fiber is tightly wrapped by particles and plays the role of "building bridges" (Figure 11c,d). The integrity of the particles is improved and the pores decrease. Hence, the strength increases through physical action. The whole is presented as an "attached skeleton". The schematic diagram shows in Figure 12c.

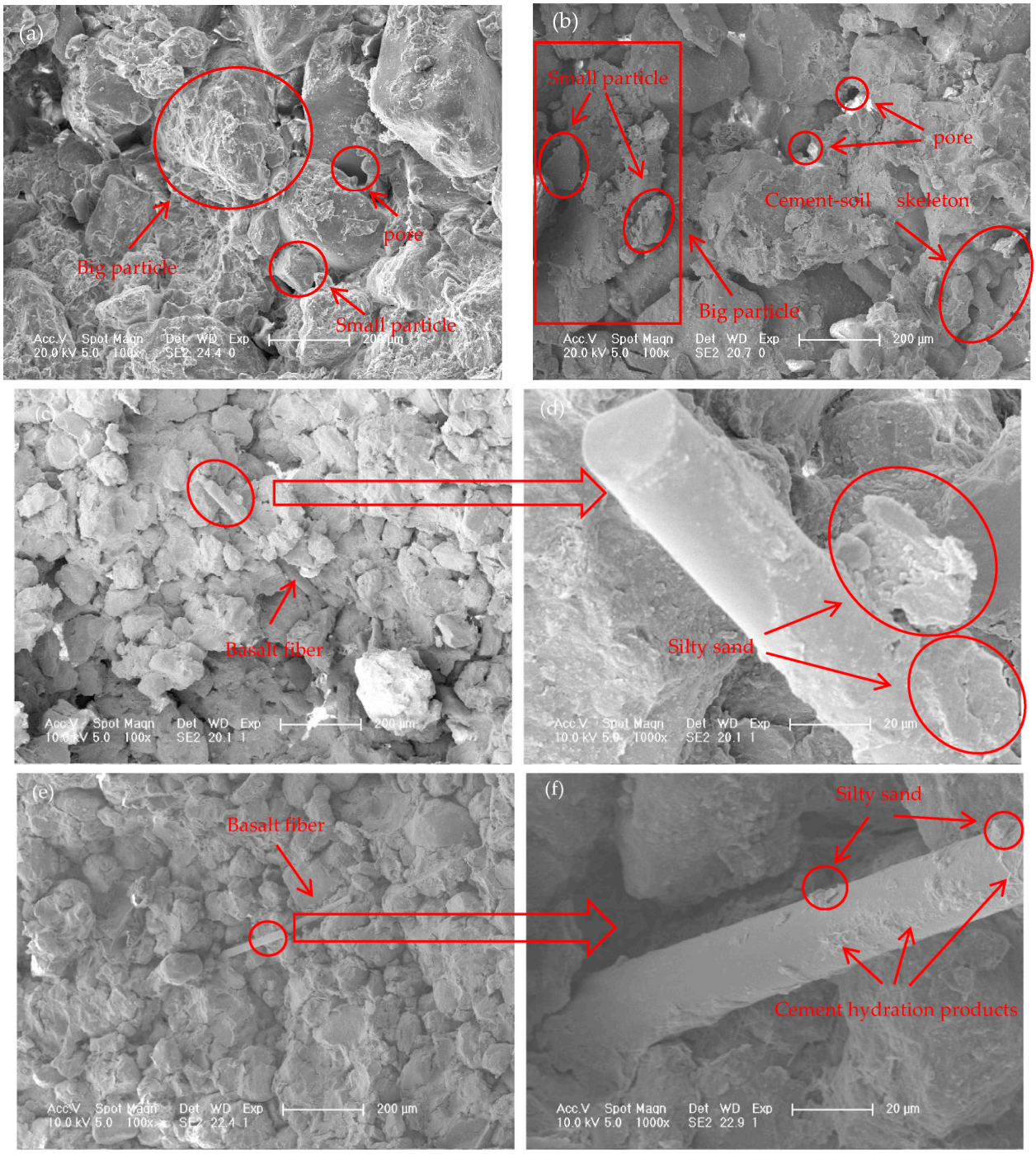

Figure 11. SEM images of typical samples: (**a**) SM0B magnified 100×, (**b**) SM2P0B magnified 100×, (**c**) SM0.2B magnified 100×, (**d**) local marked magnified area of (**c**) (1000×), (**e**) SM2P0.2B magnified 100×, and (**f**) local marked magnified area of (**e**) (1000×).

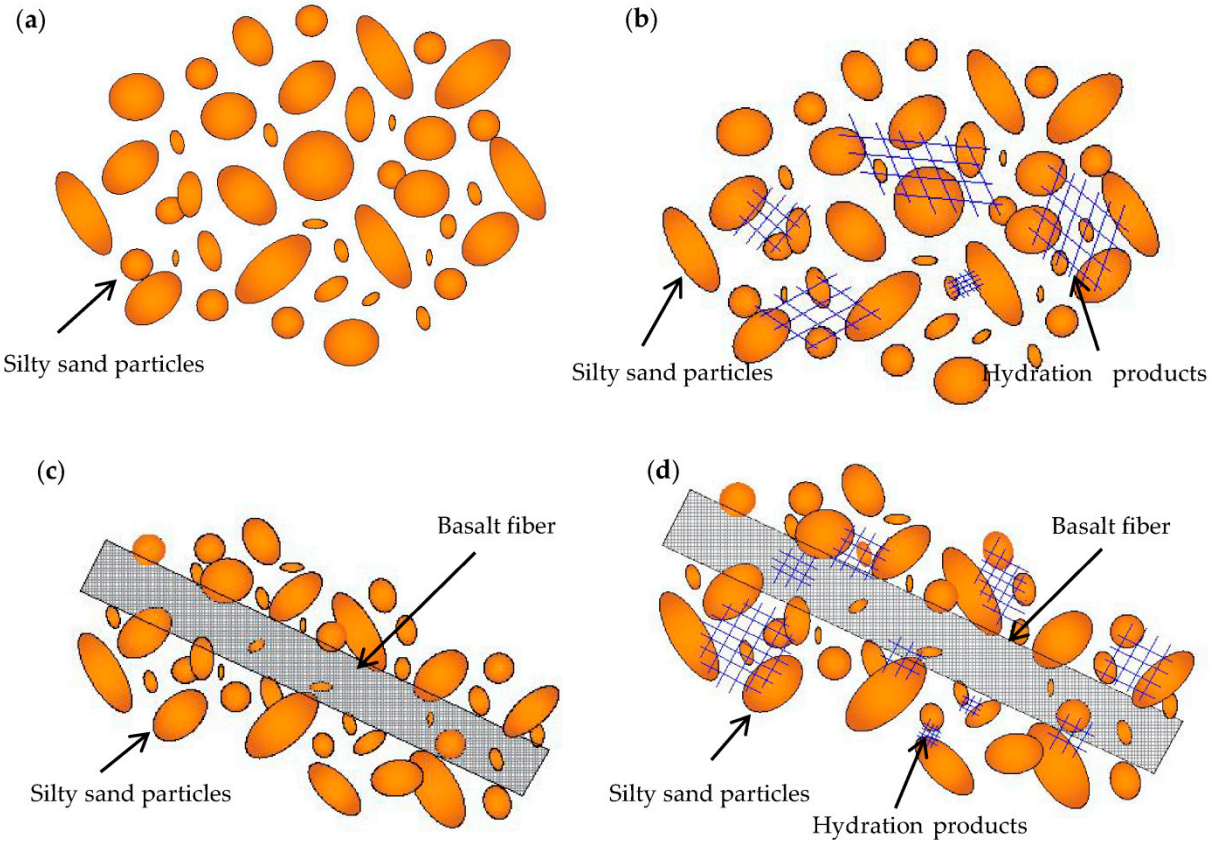

Figure 12. The microscopic mechanism of fiber reinforced: (**a**) SM0B, (**b**) SM2P0B, (**c**) SM0.2B and (**d**) SM2P0.2B.

Figure 11b shows that the soil relies on the cement-soil skeleton formed by the hydration reaction to provide strength after the cement is incorporated. The particles have good integrity, small particles attach to the surface of large particles and fill pores, pore size, and pore numbers are reduced, and the strength is significantly improved by chemical action. The structure is a "flocculation structure". The schematic diagram presents in Figure 12b.

From Figure 11e,f, after the inclusion of BF and cement, the silty sand and hydration products are both attached to the surface of the fiber together, forming a better connection in the cement-soil skeleton, which enhances the interaction between the silty sand, cement, and fiber. The particle integrity is further improved, the pores are further decreased, and the strength is further significantly improved by the combined effect of physical action and chemical action. The whole is still presented as a "flocculation structure". The schematic diagram is shown in Figure 12d.

In summary, due to a combination of the physical action of fiber reinforcement and the chemical action of cement hydration reaction, the bonding force between particles is made larger. Furthermore, due to the existence of fiber-cement-soil skeleton structure, improve the bonding capacity between particles, therefore, the strength is enhanced.

6. Conclusions

The effect of fiber contents and curing time on q_u and q_t of BFUSM and BFCSM was analyzed on the basis of UCS tests and STS tests. Meanwhile, the developed MNLR models were established to predict the q_u and q_t of BFUSM and BFCSM. Furthermore, the fiber-reinforced mechanism was revealed by a SEM test. The most important conclusions were as follows:

1. The UCS and STS of BFUSM and BFCSM both increased as the curing time increased, which reached the maximum value after curing for 28 days. The UCS and STS of BFCSM were obviously higher than that of BFUSM or cemented silty sand;
2. The UCS and STS of BFUSM and BFCSM both increased first and then decreased with the fiber contents, and both obtained the maximum value at 0.2% dosage, which was the optimal fiber content. BF had a more significant impact on STS than that on UCS;
3. The UCS and STS of BFUSM and BFCSM both had a good linear correlation and the correlation coefficients were 0.093 and 0.149, respectively. The interaction between fiber contents and curing time on the UCS and STS was significant. The developed MNLR models had high correlation coefficients and could be used to effectively predict the q_u and q_t of BFUSM and BFCSM;
4. The microscopic mechanism of fiber reinforced cemented silty sand was attributed to the physical action of fiber reinforcement and the chemical action of cement hydration reaction to form a fiber-cement-soil skeleton structure with greater bonding capacity between particles to enhance the strength.

Author Contributions: Conceptualization, S.S. and H.L.; methodology, S.S.; validation, H.L. and C.S.; formal analysis, S.S.; investigation, L.X. and Y.S.; resources, S.S. and C.S.; data curation, L.X. and Y.S.; writing—original draft preparation, S.S.; writing—review and editing, S.S. and C.S.; visualization, Y.S.; supervision, H.L. All authors have read and agreed to the published version of the manuscript.

Funding: This study was funded by the Jilin Provincial Department of Education Scientific Research Project (JJKH20230348KJ) and the Graduate Innovation Fund of Jilin University (101832020CX155).

Institutional Review Board Statement: Not applicable.

Informed Consent Statement: Not applicable.

Data Availability Statement: The data presented in this study are available on request from the corresponding author.

Acknowledgments: The authors would like to thank the Jilin Provincial Department of Education Scientific Research Project (JJKH20230348KJ) and the Graduate Innovation Fund of Jilin University (101832020CX155). We appreciate Jilin University for providing the test instruments and equipment as well as the test site. The authors are grateful to the editor and the anonymous reviewers for their comments.

Conflicts of Interest: The authors declare no conflict of interest.

References

1. Jiang, T.; Zhao, J.; Zhang, J. Splitting tensile strength and microstructure of xanthan gum-treated loess. *Sci. Rep.* **2022**, *12*, 9921. [CrossRef]
2. Xiao, Y.; Tong, L.; Che, H.; Guo, Q.; Pan, H. Experimental studies on compressive and tensile strength of cement-stabilized soil reinforced with rice husks and polypropylene fibers. *Constr. Build. Mater.* **2022**, *344*, 128242. [CrossRef]
3. Jiang, P.; Zhou, L.; Zhang, W.; Wang, W.; Li, N. Unconfined compressive strength and splitting tensile strength of lime soil modified by nano clay and polypropylene fiber. *Crystals* **2022**, *12*, 285. [CrossRef]
4. Porcino, D.D.; Diano, V. The influence of non-plastic fines on pore water pressure generation and undrained shear strength of sand-silt mixtures. *Soil Dyn. Earthq. Eng.* **2017**, *101*, 311–321. [CrossRef]
5. Mohseni, S.; Payan, M.; Chenari, R.J. Soil-structure interaction analysis in natural heterogeneous deposits using random field theory. *Innov. Infrastruct. Solut.* **2018**, *3*, 62. [CrossRef]
6. Enomoto, T. Liquefaction and post-liquefaction properties of sand-silt mixtures and undisturbed silty sands. *Soils Found.* **2019**, *59*, 2311–2323. [CrossRef]
7. Wei, X.; Yang, J. Cyclic behavior and liquefaction resistance of silty sands with presence of initial static shear stress. *Soil Dyn. Earthq. Eng.* **2019**, *122*, 274–289. [CrossRef]
8. Shafiee, A.; Hassanipour, A.; Payan, M.; Bahmani Tajani, S.; Jamshidi Chenari, R. Analysis of the stiffness and damping characteristics of compacted sand-in-fines granular composites: A multiscale investigation. *Granul. Matter* **2022**, *24*, 87. [CrossRef]
9. Zhao, Y.; Liu, J.; Hua, L.; Kong, L.; Sang, S.; Yuan, Q. Mechanical characteristics of overconsolidated hydrate-bearing clayey–silty sediments with various confining pressure. *Acta Geotech.* 2023. [CrossRef]
10. Ng, C.W.W.; Peprah-Manu, D. Pore structure effects on the water retention behaviour of a compacted silty sand soil subjected to drying-wetting cycles. *Eng. Geol.* **2023**, *313*, 106963. [CrossRef]

11. Elert, K.; Azañón, J.M.; Nieto, F. Smectite formation upon lime stabilization of expansive marls. *Appl. Clay Sci.* **2018**, *158*, 29–36. [CrossRef]
12. Siddiqua, S.; Barreto, P.N.M. Chemical stabilization of rammed earth using calcium carbide residue and fly ash. *Constr. Build. Mater.* **2018**, *169*, 364–371. [CrossRef]
13. Muhammad, N.; Siddiqua, S. Stabilization of silty sand using bentonite-magnesium-alkalinization: Mechanical, physicochemical and microstructural characterization. *Appl. Clay Sci.* **2019**, *183*, 105325. [CrossRef]
14. Ekmen, A.B.; Algin, H.M.; Özen, M. Strength and stiffness optimisation of fly ash-admixed DCM columns constructed in clayey silty sand. *Transp. Geotech.* **2020**, *24*, 100364. [CrossRef]
15. Paulo, J.; Oliveira, V.; Joaquim, A.O.R. Confined and unconfined behavior of a silty sand improved by the enzymatic biocementation method. *Transp. Geotech.* **2020**, *24*, 100400. [CrossRef]
16. Islam, M.S.; Elahi, T.E.; Shahriar, A.R.; Mumtaz, N. Effectiveness of fly ash and cement for compressed stabilized earth block construction. *Constr. Build. Mater.* **2020**, *255*, 119392. [CrossRef]
17. Elahi, T.E.; Shahriar, A.R.; Alam, K.; Abedin, Z. Effectiveness of saw dust ash and cement for fabrication of compressed stabilized earth blocks. *Constr. Build. Mater.* **2020**, *259*, 120568. [CrossRef]
18. Elahi, T.E.; Shahriar, A.R.; Islam, M.S.; Mehzabin, F.; Mumtaz, N. Suitability of fly ash and cement for fabrication of compressed stabilized earth blocks. *Constr. Build. Mater.* **2020**, *263*, 120935. [CrossRef]
19. Ayeldeen, M.; Kitazume, M. Using fiber and liquid polymer to improve the behaviour of cement-stabilized soft clay. *Geotext. Geomembr.* **2017**, *45*, 592–602. [CrossRef]
20. Abdeldjouad, L.; Asadi, A.; Ball, R.J.; Nahazanan, H.; Huat, B.B.K. Application of alkali-activated palm oil fuel ash reinforced with glass fibers in soil stabilization. *Soils Found.* **2019**, *59*, 1552–1561. [CrossRef]
21. Ghadr, S.; Samadzadeh, A.; Bahadori, H.; Assadi-Langroudi, A. Liquefaction resistance of fibre-reinforced silty sands under cyclic loading. *Geotext. Geomembr.* **2020**, *48*, 812–827. [CrossRef]
22. Pham, T.A.; Dias, D. Comparison and evaluation of analytical models for the design of geosynthetic-reinforced and pile-supported embankments. *Geotext. Geomembr.* **2021**, *49*, 528–549. [CrossRef]
23. Zhao, Y.; Yang, Y.; Ling, X.; Gong, W.; Li, G.; Su, L. Dynamic behavior of natural sand soils and fiber reinforced soils in heavy-haul railway embankment under multistage cyclic loading. *Transp. Geotech.* **2021**, *28*, 100507. [CrossRef]
24. Al Hattamleh, O.; Rababah, S.; Alawneh, A.; Alqawab'ah, A. Verification of unified effective stress theory based on the effect of moisture on mechanical properties of fiber reinforced unsaturated soil. *Geotext. Geomembr.* **2021**, *49*, 976–990. [CrossRef]
25. Bao, X.H.; Huang, Y.J.; Jin, Z.Y.; Xiao, X.; Tang, W.C.; Cui, H.Z.; Chen, X.S. Experimental investigation on mechanical properties of clay soil reinforced with carbon fiber. *Constr. Build. Mater.* **2021**, *280*, 122517. [CrossRef]
26. Wang, S.; Xue, Q.; Ma, W.; Zhao, K.; Wu, Z. Experimental study on mechanical properties of fiber-reinforced and geopolymer-stabilized clay soil. *Constr. Build. Mater.* **2021**, *272*, 121914. [CrossRef]
27. Liu, J.; Chen, Z.; Kanungo, D.P.; Song, Z.; Bai, Y.; Wang, D.; Li, Y.; Qian, W. Topsoil reinforcement of sandy slope for preventing erosion using water based polyurethane soil stabilizer. *Eng. Geol.* **2019**, *252*, 125–135. [CrossRef]
28. Liu, J.; Bai, Y.X.; Song, Z.Z.; Kanungo, D.P.; Wang, Y.; Bu, F.; Chen, Z.H.; Shi, X. Stabilization of sand using different types of short fibers and organic polymer. *Constr. Build. Mater.* **2020**, *253*, 119164. [CrossRef]
29. Rybin, V.A.; Utkin, A.V.; Baklanova, N.I. Alkali resistance, microstructural and mechanical performance of zirconia-coated basalt fibers. *Cem. Concr. Res.* **2013**, *53*, 1–8. [CrossRef]
30. Sohail, M.G.; Alnahhal, W.; Taha, A.; Abdelaal, K. Sustainable alternative aggregates: Characterization and influence on mechanical behavior of basalt fiber reinforced concrete. *Constr. Build. Mater.* **2020**, *255*, 119365. [CrossRef]
31. Dvorkin, L.; Bordiuzhenko, O.; Tekle, B.H.; Ribakov, Y. A method for the design of concrete with combined steel and basalt fiber. *Appl. Sci.* **2021**, *11*, 8850. [CrossRef]
32. Piuzzi, G.P.; Scheuermann Filho, H.C.; Del Carpio, J.A.V.; Consoli, N.C. The effects of porosity, asphalt content and fiberglass incorporation on the tensile strength and resilient modulus of asphalt concrete blends. *Geotext. Geomembr.* **2021**, *49*, 864–870. [CrossRef]
33. Lu, L.; Han, F.; Qin, Y.; Wu, S.; Yuan, G.; Zhao, Q.; Doh, J.H. Experimental study of the mechanical properties of basalt fibre-reinforced concrete at elevated temperatures. *Eur. J. Environ. Civ. Eng.* **2022**, *26*, 7586–7600. [CrossRef]
34. Wang, X.; Shao, J.; Wang, J.; Ma, M.; Zhang, B. Influence of Basalt Fiber on Mechanical Properties and Microstructure of Rubber Concrete. *Sustainability* **2022**, *14*, 12517. [CrossRef]
35. Long, A.; Sun, X.; Yu, Z.; Zhang, B.; Zhang, G.; Huang, P.; Wang, J. Experimental study and mechanism analysis on the basic mechanical properties of hydraulic basalt fiber asphalt concrete. *Mater. Struct.* **2022**, *55*, 161. [CrossRef]
36. Xiao, Y.; He, X.; Evans, T.M.; Stuedlein, A.W.; Liu, H. Unconfined compressive and splitting tensile strength of basalt fiber-reinforced biocemented sand. *J. Geotech. Geoenviron.* **2019**, *145*, 04019048. [CrossRef]
37. Wang, D.X.; Wang, H.W.; Larsson, S.; Benzerzour, M.; Maherzi, W.; Amar, M. Effect of basalt fiber inclusion on the mechanical properties and microstructure of cement-solidified kaolinite. *Constr. Build. Mater.* **2020**, *241*, 118085. [CrossRef]
38. Festugato, L.; Menger, E.; Benezra, F.; Kipper, E.A.; Consoli, N.C. Fibre-reinforced cemented soils compressive and tensile strength assessment as a function of filament length. *Geotext. Geomembr.* **2017**, *45*, 77–82. [CrossRef]
39. Ndepete, C.P.; Sert, S. Use of Basalt Fibers for Soil Improvement. *Acta Phys. Pol. A* **2016**, *130*, 355–356. [CrossRef]

40. Gao, L.; Hu, G.H.; Xu, N.; Fu, J.Y.; Xiang, C.; Yang, C. Experimental Study on Unconfined Compressive Strength of Basalt Fiber Reinforced Clay Soil. *Adv. Mater. Sci. Eng.* **2015**, *2015*, 561293. [CrossRef]
41. Cao, Z.M.; Ma, Q.Y.; Wang, H.W. Effect of Basalt Fiber Addition on static-dynamic mechanical behaviors and microstructure of stabilized soil compositing cement and fly Ash. *Adv. Civ. Eng.* **2019**, *2019*, 8214534. [CrossRef]
42. *JTG 3430-2020 Test Methods of Soils for Highway Engineering*; China Communications Press: Beijing, China, 2020.
43. Liu, H.B.; Sun, S.; Wei, H.B.; Li, W.J. Effect of freeze-thaw cycles on static properties of cement stabilised subgrade silty soil. *Int. J. Pavement Eng.* **2022**, *23*, 3770–3782. [CrossRef]
44. Chen, S.L.; Hou, R.; Ni, C.L.; Wang, J.X. Research on the Mechanical Properties of Cemented Soil Based on Triaxial Compression Tests. *Bull. Chin. Ceram. Soc.* **2018**, *37*, 4012–4017.
45. Lv, X.F.; Zhou, H.Y.; Liu, X.L.; Song, Y.M. Experimental Study on the Effect of Basalt Fiber on the Shear Behavior of Cemented Sand. *Environ. Earth Sci.* **2019**, *78*, 688. [CrossRef]
46. *JTG E51-2009 Test Methods of Materials Stabilized with Inorganic Binders for Highway Engineering*; China Communications Press: Beijing, China, 2009.
47. Liu, J.; Bai, Y.; Song, Z.; Wang, Y.; Chen, Z.; Wang, Q.; Kanungo, D.P.; Qian, W. Effect of basalt fiber on the strength properties of polymer reinforced sand. *Fibers Polym.* **2018**, *19*, 2372–2387. [CrossRef]
48. Wang, S.; Chen, F.; Xue, Q.; Zhang, P. Splitting tensile strength of cement soil reinforced with basalt fibers. *Materials* **2020**, *13*, 3110. [CrossRef]
49. Tran, K.Q.; Satomi, T.; Takahashi, H. Improvement of mechanical behavior of cemented soil reinforced with waste cornsilk fibers. *Constr. Build. Mater.* **2018**, *178*, 204–210. [CrossRef]
50. Tran, K.Q.; Satomi, T.; Takahashi, H. Tensile behaviors of natural fiber and cement reinforced soil subjected to direct tensile test. *J. Build. Eng.* **2019**, *24*, 100748. [CrossRef]
51. Ahmed, A. Simplified regression model to predict the strength of reinforced sand with waste polystyrene plastic type. *Geotech. Geol. Eng.* **2012**, *30*, 963–973. [CrossRef]
52. Maliakal, T.; Thiyyakkandi, S. Influence of randomly distributed coir fibers on shear strength of clay. *Geotech. Geol. Eng.* **2013**, *31*, 425–433. [CrossRef]